SCIENCE CHINA
Chemistry

•ARTICLES•

July 2022 Vol.65 No.7: 1315–1320
https://doi.org/10.1007/s11426-022-1272-5

Covalent organic frameworks catalyzed by organic Lewis acid

Xiangqian Shi[1], Lezhi Yi[1] & Hexiang Deng[1,2,3*]

[1]*College of Chemistry and Molecular Sciences, Wuhan University, Wuhan 430072, China;*
[2]*Hubei Yangtze Memory Laboratories, Wuhan 430205, China;*
[3]*Key Laboratory of Biomedical Polymers-Ministry of Education, College of Chemistry and Molecular Sciences, Wuhan University, Wuhan 430072, China*

Received March 31, 2022; accepted May 3, 2022; published online May 25, 2022

We report the synthesis of covalent organic framework (COF) crystals with organic Lewis acid instead of the conventional use of Brønsted acid or inorganic Lewis acid. Specifically, tris(pentafluorophenyl)borane was applied for the growth of seven imine COFs: TAPB-PDA-, TAPB-2,5-DMTA-, TAPB-2,3-DMTA-, TAPT-PDA-, TAPT-2,5-DMTA-, TAPT-2,3-DMTA-COF with **hcb** topology and varied in functional groups, as well as a new one, COF-820, with **sql** topology. All these COFs were obtained at room temperature. Their high crystallinity and porosity demonstrate the versatility of the organic Lewis acid as a catalyst. Bulky organic Lewis acid was found critical for the production of COF-820, while its absence resulted in the formation of a different COF, 4PE-1P-COF, with **kgm** topology using the same building blocks. Such steric effect, typical for organic catalysts, provides a new way to regulate the topology of COFs and their future design.

covalent organic framework, organic lewis acid, tris(pentafluorophenyl)borane, topology regulation

Citation: Shi X, Yi L, Deng H. Covalent organic frameworks catalyzed by organic Lewis acid. *Sci China Chem*, 2022, 65: 1315–1320, https://doi.org/10.1007/s11426-022-1272-5

1 Introduction

Covalent organic framework is an emerging family of porous crystalline materials constructed from molecular building blocks linked by covalent bonds [1]. The crystallization of COFs with imine linkage paved the way to the recent thriving of chemically stable COFs for the separation of useful molecules, catalysis and biomedical applications [2–5]. In the conventional synthesis of imine COFs, Brønsted acids, *e.g.*, acetic acid, are usually applied as the catalysts to activate the aldehyde carbon in one of the molecular building blocks (Scheme 1a). It usually takes more than a week to obtain imine COFs with high crystallinity and requires a relatively high reaction temperature, typically more than 120 °C [6,7]. The growth process was drastically accelerated by switching Brønsted acid to inorganic Lewis acid, such as metal triflates and metal halides [8,9], where the coordination between oxygen and the metal ions further activates the aldehyde carbon (Scheme 1b). In the following step, the aldehyde carbon is attacked by an amine, which is also electrophilic [10]. The presence of both Brønsted acid and Lewis acid will also influence the attack of amine (Scheme 1b). Therefore, a delicate balance between the activation of aldehyde carbon and nucleophilic attack of amine is required for the overall formation of the imine bond during the growth of imine COFs.

Different from inorganic Lewis acid, organic Lewis acid might not be as efficient in activating aldehyde carbon because of its steric [11–13]. However, its relatively weaker influence on the amine caused by the steric effect is usually overlooked [14–18], especially in the synthesis of COFs. In this study, we use tris(pentafluorophenyl)borane (TPFB) to show that organic Lewis acid is also capable of efficient catalysts for the growth of imine COFs (Scheme 1b). A series

*Corresponding author (email: hdeng@whu.edu.cn)

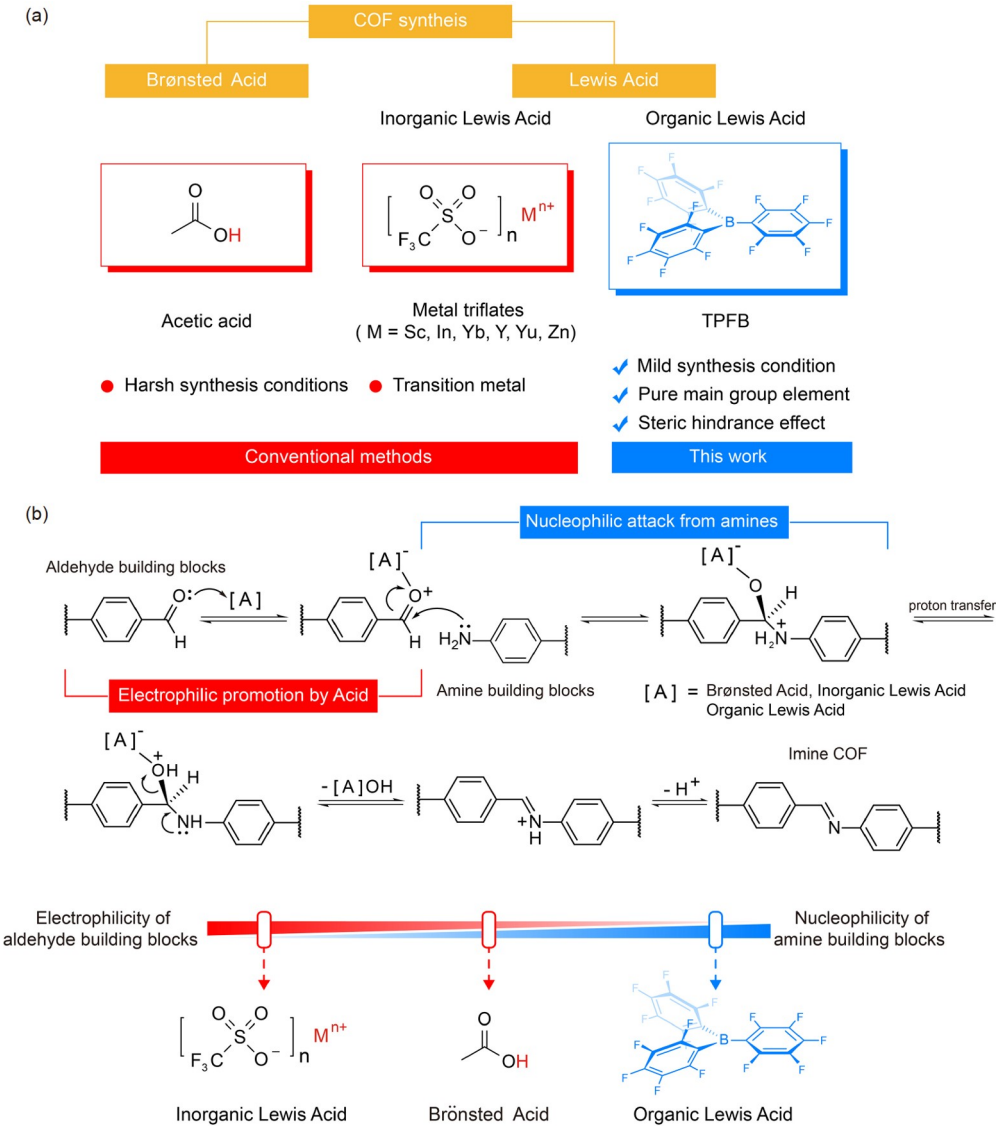

Scheme 1 (a) General comparison of conventional methods and this work for COF synthesis. (b) Comparison of Brønsted acid, inorganic Lewis acid, and organic Lewis acid from the perspective of the formation mechanism of imine COF (color online).

of COFs, TAPB-PDA-, TAPB-2,5-DMTA-, TAPB-2,3-DMTA-, TAPT-PDA-, TAPT-2,5-DMTA-, TAPT-2,3-DMTA-COF, with **hcb** topology and various functional groups (such as triazine, methoxy), was obtained by this catalyst, respectively. In addition, a new structure with **sql** topology, COF-820, was synthesized. This COF was not obtained when Brønsted acid or inorganic acid was used as catalyst [19,20]. In order to investigate the role of TPFB in the formation of COF-820, a control experiment was performed by adding extra aniline to quench this organic Lewis acid. A COF with a different topology, **kgm**, was obtained, where the majority of the pores are too small for the entrance of TPFB. This indicates that the organic Lewis acid tunes not only the formation of the imine bond, but also certain dial-in topology through the steric effect, a feature typical for organic catalysts, but not sound in Brønsted acid or inorganic Lewis acid. The versatility of this method to different functional groups and topologies makes organic Lewis acid a new tool to explore the synthesis of COFs.

2 Results and discussion

In order to demonstrate the capability of this bulky organoboron, TPFB, as an organic Lewis acid catalyst, we first selected the synthesis of TAPB-PDA-COF with **hcb** topology as an illustration (Figure 1a). The experiments were carried out under ambient conditions for three days, without applying heating or additional pressure in the conventional conditions, using Brønsted acid as a catalyst (Supporting Information online Section 2). The yellow crystals obtained were collected with a yield of about 81%. The appearance of

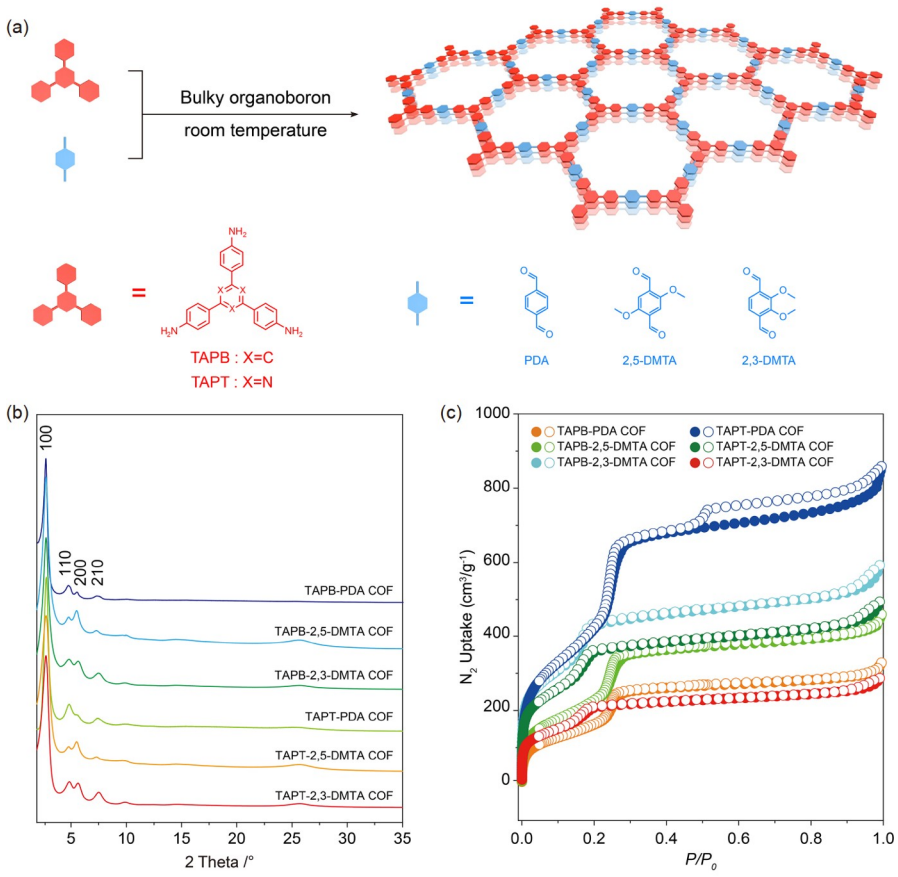

Figure 1 (a) General synthesis of bulky organoboron-catalyzed COFs and their chemical structures. (b) PXRD pattern of TAPB-PDA, TAPB-2,5-DMTA, TAPB-2,3-DMTA, TAPT-PDA, TAPT-2,5-DMTA, TAPT-2,3-DMTA-COF, respectively. (c) BET isotherms of the TAPB-PDA, TAPB-2,5-DMTA, TAPB-2,3-DMTA, TAPT-PDA, TAPT-2,5-DMTA, TAPT-2,3-DMTA-COF, respectively (color online).

a characteristic peak of C=N bond stretch at 1,624 cm^{-1} in the Fourier transform infrared (FTIR) spectrum indicates the formation of imine bonds (Figure S9). Powder X-ray diffraction (PXRD) analysis showed sharp peaks in the pattern, indicating good crystallinity. Four finger print peaks were observed at 2.80°, 4.86°, 5.58°, and 7.42°, with the corresponding *hkl* index of 100, 110, 200, and 210, respectively, confirming the successful synthesis of TAPB-PDA-COF (Figure 1b). Scanning electron microscope (SEM) images show that the product is uniform in size (around 200 nm) and pure phase (Figure S15). The organoboron catalyst was removed by washing with weak basic solvents such as acetonitrile and dioxane due to its good solubility in organic solvents prior to the activation of COF crystals. Brunauer-Emmett-Teller (BET) surface area of TAPB-PDA-COF calculated from N_2 adsorption isotherm at 77 K was 480 $m^2 g^{-1}$ (Figure 1c) in the same ball park that was synthesized using Brønsted acids as catalyst [21]. The above results show that this method offers good yield, excellent crystallinity and fair permanent porosity. In comparison to Brønsted acid, the interaction between the organoboron to the aldehyde linker was weaker. Therefore, its activation of the aldehyde was not in effect. However, COF can be synthesized under much milder conditions using organic Lewis acid. This indicates that the contribution to the catalysis originated from the reduced quench to the amine linker.

The versatility of the catalytic bulky performance of organoboron was tested by expanding the range of amine monomers and aldehyde monomers, including the less soluble triazine-based amine building blocks and methoxy-modified aldehyde building blocks. A series of COFs varied in functional groups isoreticular to TAPB-PDA-COF were obtained under the similar synthetic conditions using TPFB, namely TAPB-2,5-DMTA-, TAPB-2,3-DMTA-, TAPT-PDA-, TAPT-2,5-DMTA-, TAPT-2,3-DMTA-COF (Figure 1a), with the yield about 79%, 68%, 75%, 81%, and 76%, respectively. The FTIR spectrum shows that the characteristic peaks of C=N bond stretch appear at 1,618, 1,618, 1,621, 1,620, and 1,624 cm^{-1}, for these COFs, respectively (Figure S10-14). PXRD patterns of these COFs show the characteristic peaks at 2.8°, indicating that these COFs are identical in topology (Figure 1b). Their experimental PXRD patterns matched well with that generated from simulated structures, and the presence of sharp peaks indicated the good crystallinity of these five COFs. SEM images also confirm their uniform crystal size and phase purity (Figures

S16–S20). BET surface areas were measured, 670, 1,260, 1,280, 1,080, and 600 $m^2 g^{-1}$ for TAPB-2,5-DMTA-, TAPB-2,3-DMTA-, TAPT-PDA-, TAPT-2,5-DMTA-, TAPT-2,3-DMTA-COF, respectively, indicating their permanent porosity (Figure 1c). TAPT-PDA-COF with the triazine ring exhibited a better specific surface area compared with the Brønsted acid [22], which is likely due to the interaction between nitrogen atoms on the triazine ring and bulky organoboron. The shortened distance between the organoboron and the adjacent building blocks promotes the catalytic efficiency for the formation of imine bonds nearby. With the modification of the methoxy group on the aldehyde building blocks, its steric hindrance might affect the catalytic efficiency of the bulky organoboron, reflected in the reduced specific surface area compared with TAPT-PDA-COF. The methoxy groups present in the channel would also occupy space, therefore decreasing the pore volume (Figures S22–S26). These results demonstrated that organic Lewis acid is applied to the synthesis of COFs with different substituents.

In addition to the promotion of catalytic efficiency for COF synthesis, the bulkiness of organic Lewis acid will also offer structure tunability of COFs through steric effect, a feature yet available in Brønsted acids or inorganic Lewis acid. The topology and pore size of COFs are known to be critical for their macroscopic applications [23,24]. The topology of the resulting COF is usually determined by the symmetry of building blocks. However, in some cases, the same set of building blocks can lead to different topologies. For example, the combination of a quad-linked building block with D_{2h} symmetry, tetraphenylethene, and double-linked monomers with C_2 symmetry, terephthalaldehyde, will lead to the formation of two topologies in 2D, **sql** and **kgm** [25]. Different pore types and pore sizes are observed in the COFs with these two topologies. The COF in **kgm** topology exhibits a hierarchical pore structure containing two types of channels. One is a larger channel in hexagonal shape, accounting for only 33% of the entire pores, and the other is a smaller one in triangular shape contributing to 66%. The COF in **sql** topology displays channels of a single type in quadrilateral shape, the pore size of which is larger than that of the triangular pore in the **kgm** topology (Scheme 2).

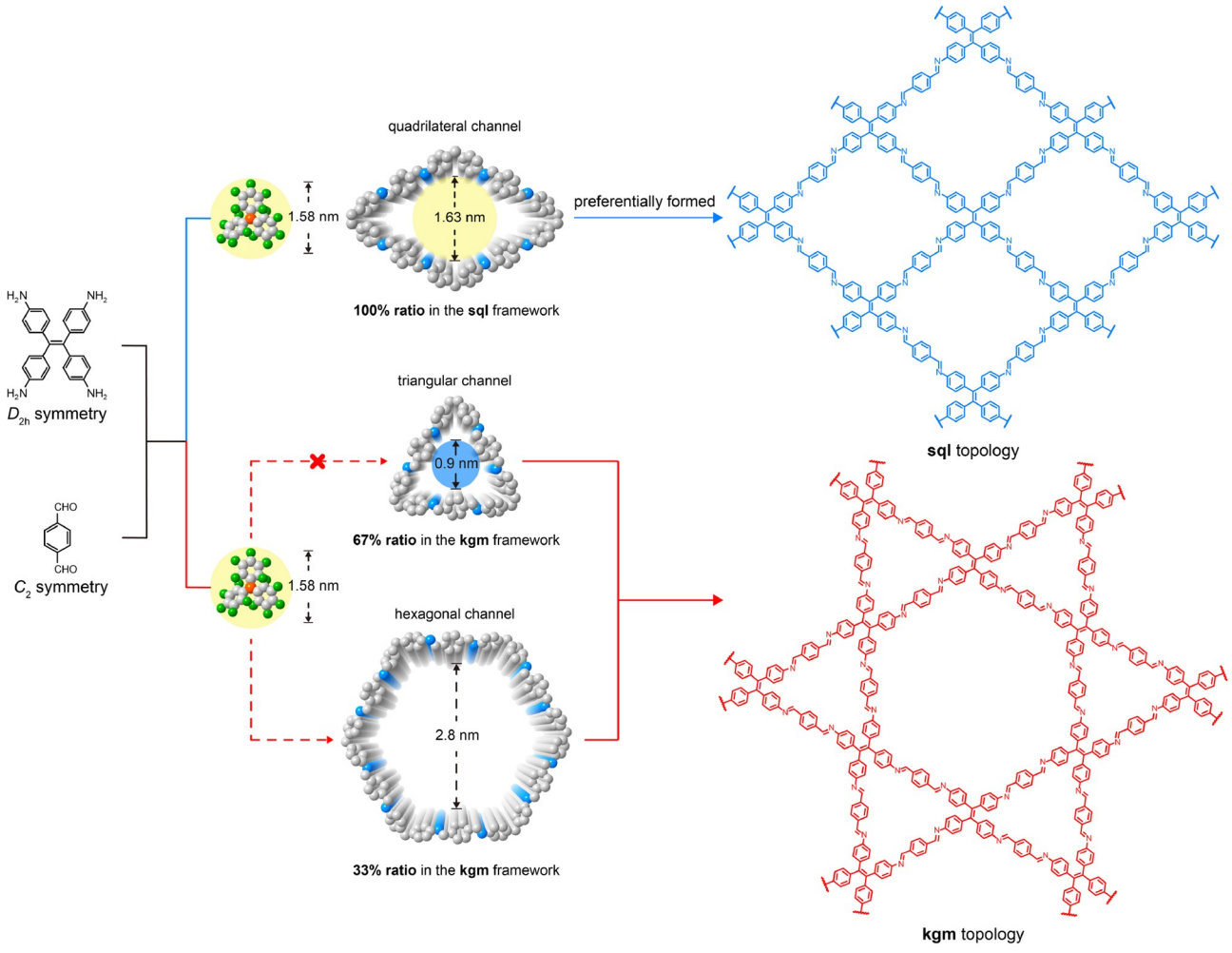

Scheme 2 Preferential formation of **sql** topology under the catalysis of bulky organoboron caused by steric effect (color online).

The difference between these two pores allows for topology regulation using bulky organoboron as a catalyst. The size of TPFB is 1.58 nm, which is smaller than the quadrangular pores in the **sql** topology but larger than the triangular pores, 0.90 nm, taking up the majority of the pores in the corresponding COF. When TPFB was used, a new COF, COF-820, in **sql** topology was obtained instead of 4PE-1P-COF, a known COF in **kgm** topology, using Brønsted acid as a catalyst. The PXRD patterns of the resulting COF show three finger print peaks, typical for **sql** topology, with the strongest at 4.85°, and the other two at 9.71° and 12.29°, respectively. These peaks matched well with the simulated structure of **sql** topology, distinctively different from those of **kgm** topology, demonstrating the phase purity (Figure 2a). The nitrogen adsorption isotherm of COF-820 shows a type I isotherm, and the single peak in pore size distribution is in good accordance with the single pore type for COF-820 (Figure S27). SEM image also shows uniform morphology with rhombic flakes (Figure 2a). The regulation of the synthesis of COF in **sql** topology is likely attributed to the fitting of the organoboron into the pores of these COFs. The quadrilateral pore in COF-820 with **sql** topology is large enough to the allowed entrance of TPFB to carry catalysis for structure formation. Although the hexagonal pore is large enough, the majority of triangular pores are too small to include TPFB inside, inhibiting the formation of 4PE-1P-COF in **kgm** topology. This unveils the potential of organic Lewis acid in controlling topology for COF synthesis.

To further verify the role of organic Lewis acid in topology regulation, control experiment with the extra amount of aniline to quench the acidic site in TPFB. As the ratio of aniline increased, a mixed phase of two topologies emerged. The PXRD pattern showed multiple peaks, corresponding to the finger print peaks of both simulated **sql** and **kgm** structures. SEM images revealed two morphologies for the product obtained from this condition, rhombic sheet and spherical structures (Figure 2c).

As aniline was added with higher proportions, the formation of COF-820 with **sql** topology was completely inhibited, resulting in the formation of 4PE-1P-COF with **kgm** topology in the pure phase. The PXRD pattern shows five finger print peaks of 4PE-1P-COF, with the highest intensity peak at 2.71°, and the other four are at 4.70°, 5.43°, 7.19° and 8.15°, respectively, corresponding to the simulated **kgm** structure (Figure 2d). The nitrogen adsorption isotherm at 77 K of 4PE-1P-COF is type IV. Two peaks were observed in

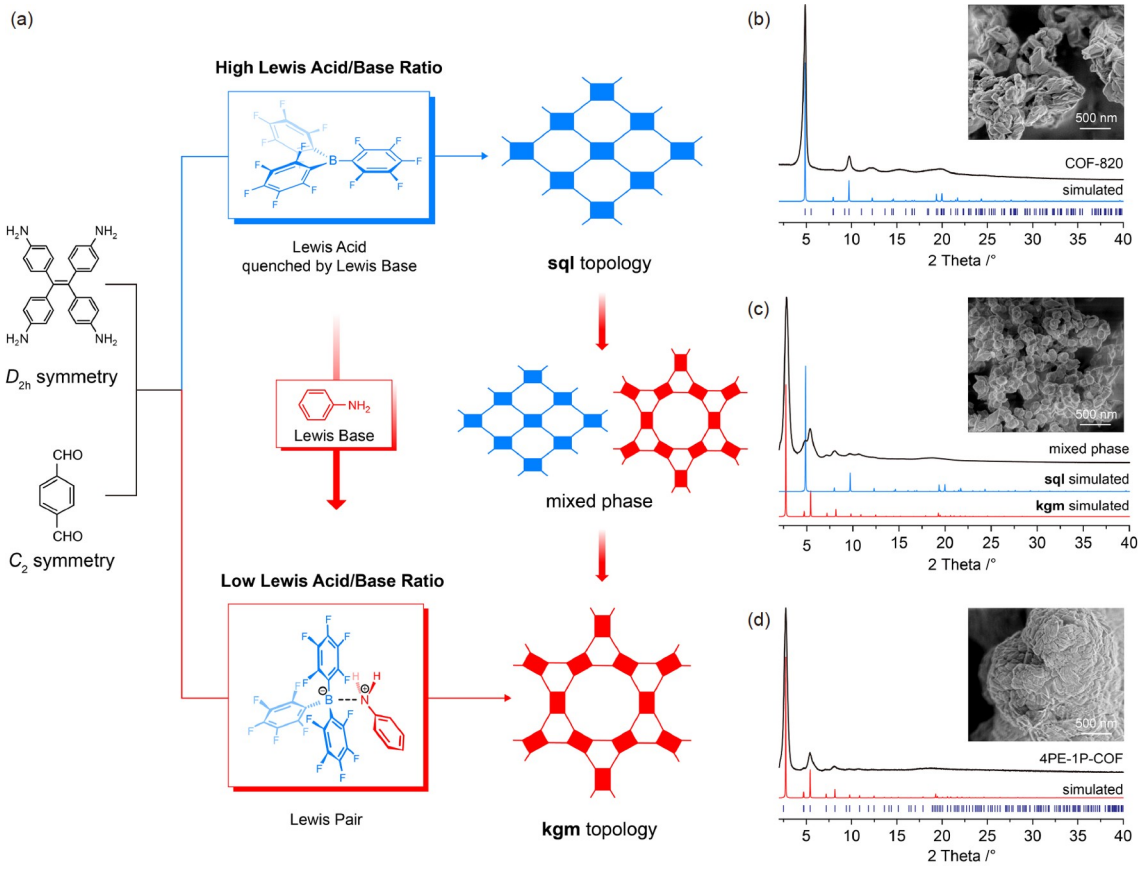

Figure 2 (a) Tuning of topology by adjusting the ratio of bulky organoboron as Lewis acids and aniline as Lewis bases. (b) Experimental (black) and simulated (blue) PXRD pattern of COF-820. Inset is the SEM image (scale bar: 500 nm) of the COF-820. (c) Experimental PXRD pattern (black) of the mixed phase of COF-820 and 4PE-1P-COF. (d) Experimental (black) and simulated (red) PXRD pattern of 4PE-1P-COF. Inset is the SEM image (scale bar: 500 nm) of the 4PE-1P-COF (color online).

pore size distribution in good accordance with the dual-pore structure of 4PE-1P-COF (Figure S29). SEM images only showed morphology typical for 4PE-1P-COF was rod-like particles in spherical aggregates (Figure 2d). This further outlined the critical role of organic Lewis acid in topology control.

3 Conclusions

In summary, we have successfully synthesized a series of COFs with high crystallinity and porosity at room temperature in the air by using the bulky organoboron as a pure organic Lewis acid catalyst. The condition using a metal-free catalyst is less in energy consumption and pollution, which is ideally suited for large-scale production of COFs. The steric hindrance offered by the organic catalyst allows for topology regulation of COFs using the same set of building blocks, which provides a new choice for the design and synthesis of new COFs.

Acknowledgements This work was supported by the National Natural Science Foundation of China (22025106, 21971199), the National Key Research and Development Project (2018YFA0704000) and the Innovation Team of Wuhan University (2042017kf0232).

Conflict of interest The authors declare no conflict of interest.

Supporting information The supporting information is available online at http://chem.scichina.com and http://link.springer.com/journal/11426. The supporting materials are published as submitted, without typesetting or editing. The responsibility for scientific accuracy and content remains entirely with the authors.

1 Diercks CS, Yaghi OM. *Science*, 2017, 355: eaal1585
2 Ding SY, Wang W. *Chem Soc Rev*, 2013, 42: 548–568
3 Guan X, Chen F, Fang Q, Qiu S. *Chem Soc Rev*, 2020, 49: 1357–1384
4 Sun T, Wei L, Chen Y, Ma Y, Zhang YB. *J Am Chem Soc*, 2019, 141: 10962–10966
5 Guan Q, Wang GB, Zhou LL, Li WY, Dong YB. *Nanoscale Adv*, 2020, 2: 3656–3733
6 Jiang J, Zhao Y, Yaghi OM. *J Am Chem Soc*, 2016, 138: 3255–3265
7 Kandambeth S, Dey K, Banerjee R. *J Am Chem Soc*, 2019, 141: 1807–1822
8 Matsumoto M, Dasari RR, Ji W, Feriante CH, Parker TC, Marder SR, Dichtel WR. *J Am Chem Soc*, 2017, 139: 4999–5002
9 Liu Y, Zhu Y, Alahakoon SB, Egap E. *ACS Mater Lett*, 2020, 2: 1561–1566
10 Giuseppone N, Schmitt JL, Schwartz E, Lehn JM. *J Am Chem Soc*, 2005, 127: 5528–5539
11 Satchell DPN, Satchell RS. *Q Rev Chem Soc*, 1971, 25: 171–199
12 Ashley AE, Herrington TJ, Wildgoose GG, Zaher H, Thompson AL, Rees NH, Krämer T, O'Hare D. *J Am Chem Soc*, 2011, 133: 14727–14740
13 Beckett MA, Strickland GC, Holland JR, Sukumar Varma K. *Polymer*, 1996, 37: 4629–4631
14 Braunschweig H, Krummenacher I, Légaré MA, Matler A, Radacki K, Ye Q. *J Am Chem Soc*, 2017, 139: 1802–1805
15 Légaré MA, Pranckevicius C, Braunschweig H. *Chem Rev*, 2019, 119: 8231–8261
16 Welch GC, San Juan RR, Masuda JD, Stephan DW. *Science*, 2006, 314: 1124–1126
17 Welch GC, Stephan DW. *J Am Chem Soc*, 2007, 129: 1880–1881
18 Stephan DW. *J Am Chem Soc*, 2015, 137: 10018–10032
19 Zhou TY, Xu SQ, Wen Q, Pang ZF, Zhao X. *J Am Chem Soc*, 2014, 136: 15885–15888
20 Ascherl L, Sick T, Margraf JT, Lapidus SH, Calik M, Hettstedt C, Karaghiosoff K, Döblinger M, Clark T, Chapman KW, Auras F, Bein T. *Nat Chem*, 2016, 8: 310–316
21 Smith BJ, Overholts AC, Hwang N, Dichtel WR. *Chem Commun*, 2016, 52: 3690–3693
22 Gomes R, Bhanja P, Bhaumik A. *Chem Commun*, 2015, 51: 10050–10053
23 Wang K, Kang X, Yuan C, Han X, Liu Y, Cui Y. *Angew Chem Intl Ed*, 2021, 60: 19466–19476
24 Wang X, Han X, Cheng C, Kang X, Liu Y, Cui Y. *J Am Chem Soc*, 2022, 144: 7366–7373
25 Pang ZF, Zhou TY, Liang RR, Qi QY, Zhao X. *Chem Sci*, 2017, 8: 3866–3870